Proceedings of the 2nd International Conference on Computing Innovation and Applied Physics (CONF-CIAP 2023)
DOI: 10.54254/2753-8818/5/20230597

First Measurement of Extreme Ultraviolet Dust Extinction Curve in Quasars

Jinbin Liao[1], Ruohan Hamilton Guan[2], Tuo Ji[3,4]

[1]Raffles American School, Iskandar Puteri, Johor, Malaysia
[2]Yew Chung International School of Beijing, Beijing, China
[3]University of Science and Technology of China, Anhui, China

[4] tji@mail.ustc.edu.cn

Abstract. Dust is a ubiquitous feature of the cosmos, impinging directly or indirectly on most fields of modern astronomy. Dust grains composed of small (submicron-sized) solid particles pervade interstellar space in the Milky Way and other galaxies: they occur in a wide variety of astrophysical environments, ranging from comets to giant molecular clouds, from circum-stellar shells to galactic nuclei. The study of this phenomenon is a highly active and topical area of current research. Dust absorbs optical and Ultraviolet (UV) photons and re-emit them in the infrared. The heating and cooling of dust interact with their environment closely. Dust is closely related to the star formation process, and study on dust could put constraints on the star formation history. While extensively studied in the optical, the extinction property of dust in the UV is still an open question. UV photos are absorbed by earth atmosphere and cannot be accessed from ground-based observations. NASA space mission Galaxy Evolution Explorer (GALEX), on the other hand, provides critical data to this question by surveying the whole sky in two UV bands. By comparing the optical and UV properties of blue and red (dust-absorbed) quasars selected from Sloan Digital Sky Survey (SDSS), we shape the extreme UV dust extinction curve for the first time. The measured UV dust extinction curve will help us characterize the size distribution of dust grains and their compositions which could not be easily accessed by other methods.

Keywords: quasars, EUV extinction curve, ISM

1. Introduction

Dust is present almost everywhere in the universe. Though only < 0.01% of matter in galaxies is composed of dust, the combined effects of extinction, scattering, and re-emitted thermal radiation of dust have a profound impact on our view of the universe. The effect is mainly seen in the optical/UV band as extinction and in the IR band as emission. A precise extinction curve is needed to correct for the effects of interstellar extinction and to constrain the grain size distribution and chemical composition of dust itself. Interstellar extinction curve is commonly obtained through "pair method" by comparing the spectra of two stars of the same spectral type, one of which is reddened and the other unreddened. However, when it comes to extreme UV band (< 1000 Å, hereafter EUV band), this method is very limited. First, SED (Spectral Energy Distribution) of early type O B stars don't have enough flux in the EUV band; second, EUV band suffers from severe absorption of neutral hydrogen in the ISM (Interstellar Medidum), thus reddened and even unreddened objects can easily fall below the detection

DOI: 10.54254/2753-8818/5/20230597

limit in the EUV band, either photometrically or spectroscopically. On the other hand, quasars have an SED extending 11 order of magnitude from γ ray to radio wave, rather flat continuum shape in the optical-UV band makes them easily detected in the EUV band, furthermore high luminosity of quasar up to 10^{48} ergs $s^{-1}cm^{-2}Å^{-1}$ makes it detectable at a redshift as high as 6, redshift effect makes rest-frame UV band of quasars fall in observed optical and infrared bands, which are more sensitive than current UV instruments. These effects combined make it possible to use "pair method" to infer extinction curve in quasars.

The extinction effect is strong in type 2 AGN (Active Galactic Nucleus), but weaker effect is seen in type 1 objects as well. Color distribution of SDSS quasars has revealed the existence of a significant population of red quasars [1,2]. The Gaussian distribution of red color $\Delta(r^* - i^*)$ and $\Delta(r^* - z^*)$ of their sample combined with an asymmetric red tail in the distribution of blue color $\Delta(g^* - i^*)$ strongly suggest that dust reddening is responsible for the quasars in the red tail.

It's already been argued that the properties of the dust in the extreme conditions of quasars are not similar to the dust properties in the interstellar medium of our Galaxy. Optical-UV extinction curve has been inferred by various authors through composite quasar spectra [3,4], and individual reddened AGNs [5-8]. Basically, these are done by taking the differences in spectra or magnitudes between blue and red objects. Although still there exists some debate, Little or lack of the 2175 Å bump (however, see a literature written by Zhou et al. for a quasar with super-strong 2175 Å bump) and a flatter extinction curve in optical-UV band compared with SMC (Small Magellanic Cloud) seems common in AGN and quasar spectra [9]. This puts strong constraints on dust models [10-12]. in which the composition, size and morphology of the dust determine the extinction curve and emission in IR band. However, all previews studies concentrate on optical-UV band because of lack of EUV data, where the extinction curve is more sensitive to the distribution of very small dust grains. In this paper we use GALEX photometric data to determine the EUV extinction curve of a reddened quasar sample selected by SDSS $\Delta(g^* - i^*)$ color. We select respectively blue and red SDSS quasars with GALEX observation, and create composite spectra of blue and red sample. By comparing the SED of blue and red quasars, we aim to obtain EUV extinction curve experimentally for the first time.

The paper is organized as follows. In section 2, we select red and blue quasars from SDSS DR16 quasar catalog. In section 3, we construct composites for blue and red quasars and make dust extinction curve for each redshift bin. In section 4, we discuss the implication of the result. And finally, we conclude our findings in Section 5.

2. Selection of blue and red quasars

We use the final Sloan Digital Sky Survey IV (SDSS-IV) quasar catalog from Data Release 16 of the extended Baryon Oscillation Spectroscopic Survey (eBOSS). This catalog (hereafter DR16Q) comprises the largest selection of spectroscopically confirmed quasars to date, with a total of 750414 quasars [13].

DR16Q also includes force-photometered or cross-matched data from the Galaxy Evolution Explorer [14]. In the past SDSS quasar catalog, DR16Q contains data from GALEX Data Release 5, with force-photometer measurements at the location of the SDSS DR8 imaging sources [15]. DR16Q includes both GALEX bands: NUV (1350–1750 A) and FUV (1750–2750 A). A total of 646,041 objects have a nonzero flux in either the NUV or FUV band, 552,025 (431,431) have a positive NUV (FUV) flux, and 386,642 objects have a positive flux in both bands. All fluxes are reported in nanomaggies, where 1 nanomaggy 3.631×10^6 Jy.

Broad absorption line quasars (BALs) are with broad and deep absorption lines in UV bands, and their effect on spectra and photometry are potentially mixed up with dust. To avoid contamination, we first exclude them by requiring "BAL PROB" column in DR16 catalog less than zero, this result in 643359 quasars.

Also, we select targets with both SDSS and Galex Photometry, by requiring GALEX MATCHED=1 and FUV>0 and NUV>0 in DR16 catalog. This step results in 345943 quasars as our parent sample.

DOI: 10.54254/2753-8818/5/20230597

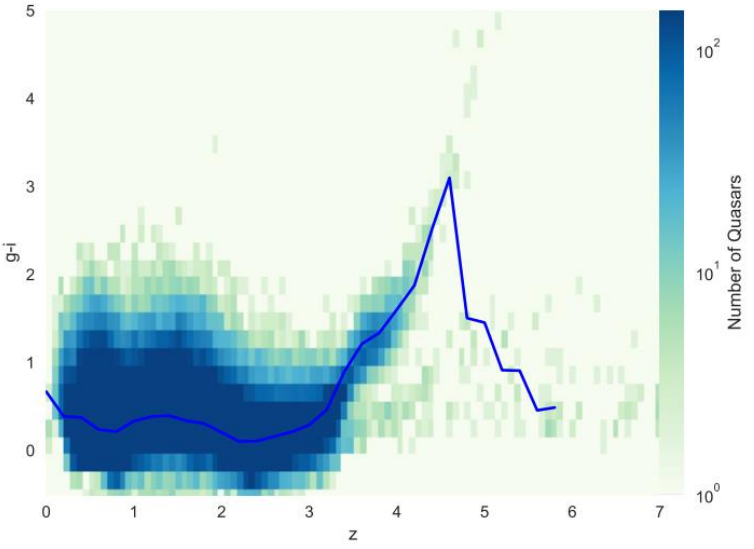

Figure 1. g-i color as function of redshift for SDSS DR16 quasars. The blue curve is the median g-i in each redshift bin of Δz=0.1. The distribution of g-i around the medians is clearly biased to larger values, indicating an excess of reddened quasars.

The g-i colors of the parent samples is shown in Figure 1 as function of redshift. Median g-i colors are also calculated in redshift bins of 0.1. The distribution of g-i around the medians is clearly biased to larger values, indicating an excess of reddened quasar. The trend is more clearly demonstrated in relative color distribution of in Figure 2 for redshift bin $1.0 < z < 1.2$. Relative color distribution is defined as $\Delta(g-i) = (g-i) - (g-i)_{median}$, i.e. the colors referenced to the median color at a given redshift bin as in Richards et al. (2001) [1].

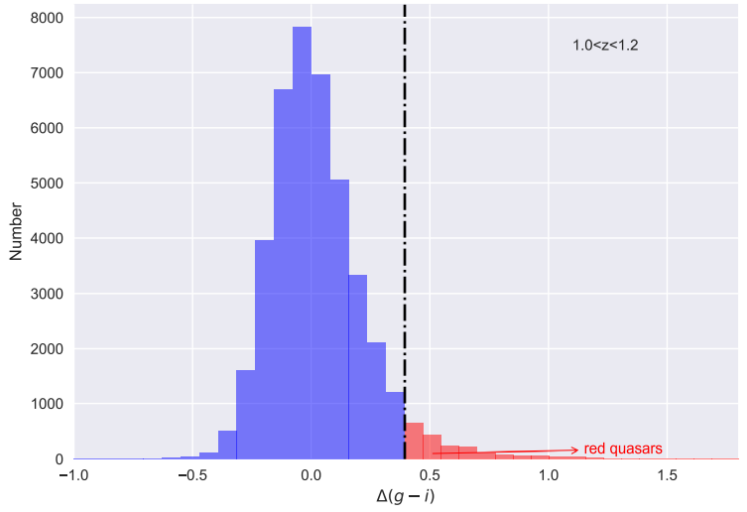

Figure 2. Relative color distribution Δ(g-i) of the quasars in the redshift bin of 1.0<z<1.2. The profile is Gaussian like except for a red tail excess. The dot dashed line indicate the sigma of the Guassian Profile of 0.4, calculated for the blue part of the profile.

As can be seen, there is an obvious red tail in the distribution of this redshift bin as well as other redshift bins defined in Section 3, from which we recover our red quasar population. To define the red population unbiasedly, we first fit the peak and blue wing of the distribution for each redshift bins with a Gaussian profile, then according to this profile we draw sources randomly from the red wing of the

DOI: 10.54254/2753-8818/5/20230597

distribution. This procedure generates 14856 sources whose distribution is Gaussian like. The remaining 1000 sources are considered as dust reddened quasars. We then use $\Delta(g^* - i^*) > 0.3$ to set a minimum amount of reddening [2]. This yields our final sample of 860 reddened quasars. The redshift and magnitude distribution of the blue and red samples in this redshift bin are shown in Figure 3. We perform similar operation to select red and blue samples on all the redshift bins defined in Section 3 and construct composites for blue and red samples.

3. Construction of extinction curve

Traditionally, the method use to determine the wavelength dependent extinction, known as extinction curve, is the "pair method" which is constructed by comparing the fluxes of a reddened object and an identical unreddened object. In AGN context, the comparison is made between red and blue quasars, either individuals or composites. Our aim is to determine the EUV extinction curve with the addition of photometric data of GALEX. The effective central wavelengths of GALEX FUV and NUV band are 1539 Å and 2316 Å, respectively, while SDSS u^*, g^*, r^*, i^*, z^* filters are centered at 3551 Å, 4686 Å, 6166 Å, 7480 Å, 8932 Å.

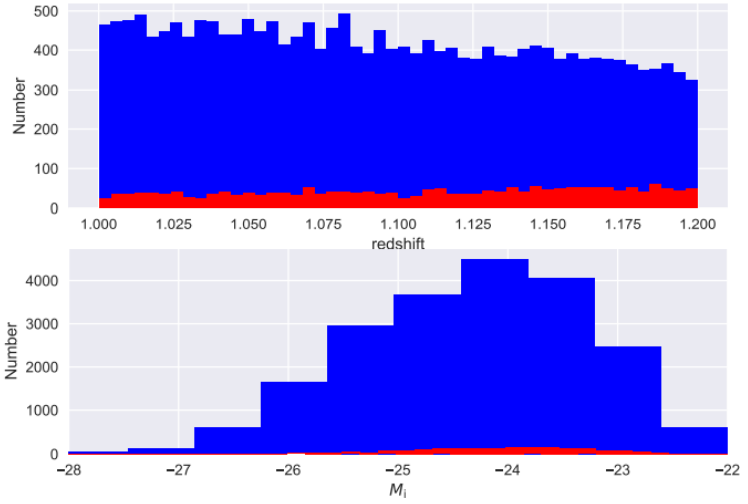

Figure 3. Magnitude and redshift distributions of red and blue samples in the redshift bin of 1.0<z<1.2.

With careful choosing of redshift bins, we could in principle determine the SED from 500 Å in extreme UV band to 5000 Å in optical band. In practice, we use redshift bins of $1.0 \leq z \leq 1.2$, $1.2 \leq z \leq 1.4$, $1.4 \leq z \leq 1.6$, $1.6 \leq z \leq 1.8$, $2.0 \leq z \leq 2.2$, $2 \leq z \leq 2.2$. The chosen redshift ranges ensure the required wavelength coverage and relatively uniform distribution of the rest-frame center wavelengths of the 7 filters. The redshift ranges are also chosen to be relatively narrow so that there is no strong evolution in the dust properties of the quasars in each redshift bin and mean redshift of quasars in each bin could be used. The i band magnitude distribution of reddened quasars is shown as red lines in bins of $\delta M_i = 0.5$ in Figure 3, while unreddened as blue lines. To minimize the possible effect that spectral shape is correlated with luminosity, we make sure the blue sample has the same magnitude distribution as the red one. In each bin of red quasar magnitude distribution, we select 10 times the number of red ones from the blue sample. We make mean composite spectra for both blue and red quasars in each redshift bin using the same method described in a literature published by Vanden Berk et al. [16]. A two-sided KS test between the redshift and magnitude distributions of the blue and red samples suggests that the two distributions are drawn from the same underlying distribution. The composites for redshift bin $1.0 < z < 1.2$ are shown in Figure 4. As previous literature have pointed out, an SMC-type extinction causes the difference between red and blue composites [2]. We fit composite ratio spectra (blue spectrum in Figure 4) in each redshift bin with the following equation:

DOI: 10.54254/2753-8818/5/20230597

$$\frac{\mathrm{f_{blue}}}{\mathrm{f_{red}}} = \mathrm{C} * 10.0^{0.4*\mathrm{k(x)}*\mathrm{E(B-V)}} \tag{1}$$

where $k(x)$ is the SMC-type extinction curve, $k(x) = A(x)/E(B-V) = 1.39 \cdot x^{1.2}$, x is wave number define as $1/\lambda$ (μm^{-1}), C is a normalization factor to account for the scaling of individual quasars during the construction of composite. The fit is quite good, as shown in Figure 4 for redshift bin $1.0 < z < 1.2$. we get color excess $E(B-V)$ for each redshift bin.

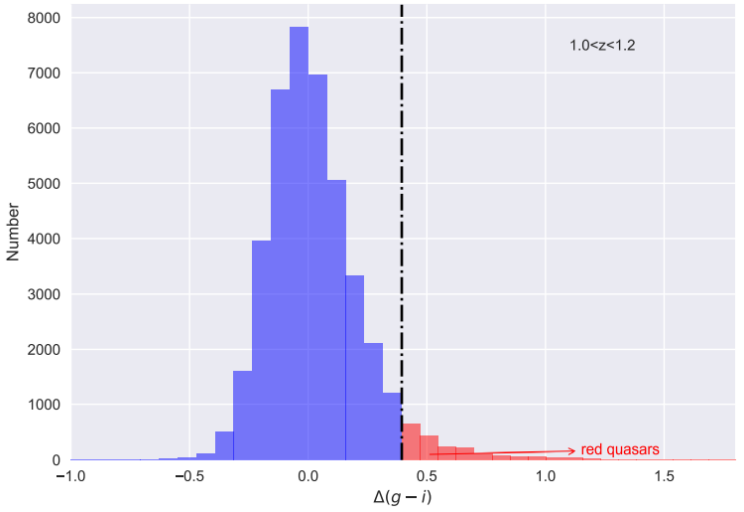

Figure 4. Relative color distribution Δ(g-i) of the quasars in the redshift bin of 1.0<z<1.2. The profile is Gaussian like except for a red tail excess. The dot dashed line indicate the sigma of the Guassian Profile of 0.4, calculated for the blue part of the profile.

We then use the fitted values of C and $E(B-V)$ to normalize the flux ratios between blue-to-red composite and blue-to-red photometries. This procedure produces the average extinction curve for each redshift bin, as

$$A(x) = -2.5 \log_{10} \frac{\left(\frac{f_{blue}}{C * f_{red}}\right)}{E(B-V)} \tag{2}$$

DOI: 10.54254/2753-8818/5/20230597

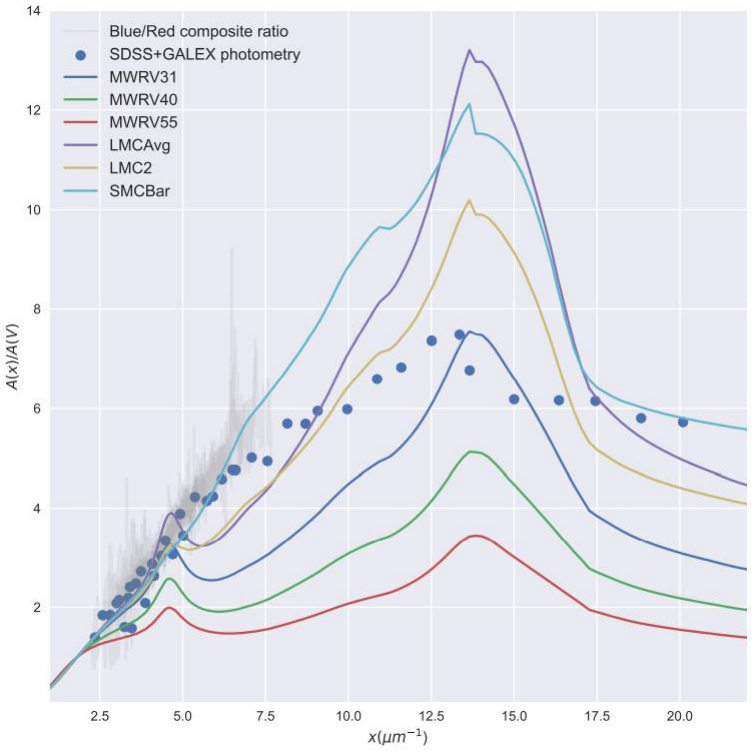

Figure 5. Relative color distribution Δ(g-i) of the quasars in the redshift bin of 1.0<z<1.2. The profile is Gaussian like except for a red tail excess. The dot dashed line indicate the sigma of the Guassian Profile of 0.4, calculated for the blue part of the profile.

4. Discussion

Mathis et al. constructed their classic interstellar dust model (hereafter MRN) incorporating both silicate and graphite grains [17]. MRN found that the extinction curve is well reproduced if the grain-size distribution is in power-law form with an index of -3.5, and grain sizes are between 50 Å and 0.25 μm^{-1}. Since the development of the model, more observational evidence has become available to require revisions of the model. In a literature written by Weingartner and Draine, a new population of very small carbonaceous grains was added to improve MRN model, which is required to generate the observed IR emission from the diffuse ISM [18]. Li and Drained proposed that the very small grain population is the sum of two log-normal size distributions, with peaks at 3.5 Å and 30 Å [19].

Weingartner and Draine's result fit the continuous extinction between $0.35 < x < 8$ μm^{-1} [18]. As the authors pointed out, the lower limit of 0.35 μm^{-1} was chosen so as to avoid infrared absorption features, most notably the C-H stretch feature. However, the structure of the size distribution for the very small carbonaceous grains has only a mild effect on the extinction for the wavelengths of interest, due to the limited extinction data for $x > 8$ μm^{-1}. Thus, the exact form, as well as the amount of the population is still not clear.

Although neutral H gas is opaque at wavelengths smaller than the Lyman limit, extinction by dust at such wavelengths may yield important observations in the region of ionization, which is exactly the case in the vicinity of quasars. The combination of SDSS and GALEX data enables the EUV extinction curve in this work to extend to a wavenumber as blue as $x > 20$. This may provide the critical observational constraint on the proposed small grain population, since extinctions at short wavelengths are mostly contributed by small grains with sizes comparable with these wavelengths.

From Figure 5, we see there is a decrease after the far UV rise of the extinction curve, forming a local peak at a wavenumber of 13 ± 0.5 μm^{-1}. The position of the peak is compared with the model predictions in Weingartner and Draine's paper, which are overplotted in Figure 5 for the Milky way

DOI: 10.54254/2753-8818/5/20230597

with different RV of 3.1, 4.0 and 5.5, LMC and SMC [18]. The experimental result is consistent with the model predictions in the sense of the peak position. However, the slopes on both sides of the peak as well as the peak strength are distinctive with either of these models. This could be due to the different nature of quasar environment compared to Galaxy and Magellanic Clouds. Also, as pointed out before, the models are not well constrained in this wavelength range for Galaxy and Magellanic Clouds due to a lack of EUV extinction data. Although detail is beyond the scope of the paper, the much shallower slope beyond the peak at $x > 13 \pm 0.5$ μm^{-1} implies a more significant population of small grains in quasars, future theoretical work on our observed EUV extinction curve will help to address the small grain population in detail.

Lyα forest could potentially affect the spectral region blueward of Lyman limit at 912 Å. In addition to the accumulated absorption of "The Lyman Valley", there is random absorption by the intervening Lyman Limit Systems, which cut off the flux significantly. All the quasar's lines of sight ($z > 2$) are significantly affected by these systems. Our selected range of redshift is lower and suffers much less Lyα forest absorption than high redshift, but the effect would be still non-trivial [20]. However, the similarities in the redshift and magnitude distribution of the blue and red samples indicate no other bias on the two populations except for the intrinsic differential dust contents. The Lyα forest systems in the sightlines of the two samples should be randomly distributed and are similar to each other. Thus, the effects of the Lyα systems on the two samples are similar and canceled out during the construction of the extinction curve.

5. Conclusions

We experimentally studied the extreme-UV extinction curve of quasars for the first time. We found a significant drop after the FUV rise of the extinction curve. The result is in general agreement with the prediction of Weingartner and Draine's model, extended beyond Lyman limit, the slopes in the vicinity of the peak as well as the peak strength differ with their models, indicating very small grains have different properties than our Galaxy and Magellanic clouds, probably due to strong UV continuum of quasars [18]. Detailed modeling of the measured extinction curve will help to constrain the detailed size distribution of the dust, as well as shedding light on grain compositions and their optical properties.

References

[1] Richards, G. T., Fan, X., Schneider, D. P., et al. 2001, AJ, 121, 2308. doi:10.1086/320392
[2] Richards, G. T., Hall, P. B., Vanden Berk, D. E., et al. 2003, AJ, 126, 1131. doi:10.1086/377014
[3] Czerny, B., Li, J., Loska, Z., et al. 2004, MNRAS, 348, L54. doi:10.1111/j.1365-2966.2004.07590.x
[4] Gaskell, C. M., Goosmann, R. W., Antonucci, R. R. J., et al. 2004, ApJ, 616, 147. doi:10.1086/423885
[5] Crenshaw, D. M., Kraemer, S. B., Bruhweiler, F. C., et al. 2001, ApJ, 555, 633. doi:10.1086/321522
[6] Crenshaw, D. M., Kraemer, S. B., Turner, T. J., et al. 2002, ApJ, 566, 187. doi:10.1086/338058
[7] Maiolino, R., Schneider, R., Oliva, E., et al. 2004, Nature, 431, 533. doi:10.1038/nature02930
[8] Gaskell, C. M. & Benker, A. J. 2007, arXiv:0711.1013. doi:10.48550/arXiv.0711.1013
[9] Zhou, H., Ge, J., Lu, H., et al. 2010, ApJ, 708, 742. doi:10.1088/0004-637X/708/1/742
[10] Laor, A. & Draine, B. T. 1993, ApJ, 402, 441. doi:10.1086/172149
[11] Maiolino, R., Marconi, A., Salvati, M., et al. 2001, A&A, 365, 28. doi:10.1051/0004-6361:20000177
[12] Maiolino, R., Marconi, A., & Oliva, E. 2001, A&A, 365, 37. doi:10.1051/0004-6361:20000012
[13] Lyke, B. W., Higley, A. N., McLane, J. N., et al. 2020, ApJS, 250, 8. doi:10.3847/1538-4365/aba623
[14] Martin, C. & GALEX Team 2005, Multiwavelength Mapping of Galaxy Formation and Evolution, 197. doi:10.1007/10995020 30

DOI: 10.54254/2753-8818/5/20230597

[15] Aihara, H., Allende Prieto, C., An, D., et al. 2011, ApJS, 193, 29. doi:10.1088/0067-0049/193/2/29 Gaskell, C. M., Goosmann, R. W., Antonucci, R. R. J., et al. 2004, ApJ, 616, 147.
[16] Vanden Berk, D. E., Richards, G. T., Bauer, A., et al. 2001, AJ, 122, 549. doi:10.1086/321167
[17] Mathis, J. S., Rumpl, W., & Nordsieck, K. H. 1977, ApJ, 217, 425. doi:10.1086/155591
[18] Weingartner, J. C. & Draine, B. T. 2001, ApJ, 548, 296. doi:10.1086/318651
[19] Li, A. & Draine, B. T. 2001, ApJL, 550, L213. doi:10.1086/319640
[20] Savaglio, S., Ferguson, H. C., Brown, T. M., et al. 1999, ApJL, 515, L5. doi:10.1086/311963